ADVANCED MATERIALS
www.advmat.de

Bistable Spin-Crossover Nanoparticles for Molecular Electronics

*Ramón Torres-Cavanillas, Miguel Gavara-Edo, and Eugenio Coronado**

The field of spin-crossover complexes is rapidly evolving from the study of the spin transition phenomenon to its exploitation in molecular electronics. Such spin transition is gradual in a single-molecule, while in bulk it can be abrupt, showing sometimes thermal hysteresis and thus a memory effect. A convenient way to keep this bistability while reducing the size of the spin-crossover material is to process it as nanoparticles (NPs). Here, the most recent advances in the chemical design of these NPs and their integration into electronic devices, paying particular attention to optimizing the switching ratio are reviewed. Then, integrating spin-crossover NPs over 2D materials is focused to improve the endurance, performance, and detection of the spin state in these hybrid devices.

1. Introduction

Memory devices, including hard, solid-state, and universal serial bus (USB) drives, are essential to our daily life. Enhancing their performance is one of the most targeted scientific and commercial challenges nowadays. In this context, molecular electronics offers an elegant tool to miniaturize these devices, reaching the nanoscale or even the single-molecule level.[1,2]

The so-called spin crossover (SCO) molecules provide an appealing example of molecular bistability. Assemblies based on these magnetic molecules have centered the attention on molecular magnetism for more than 40 years as they provide unique examples of multifunctional and stimuli-responsive materials.[3] These compounds are based on $3d^n$ ($4 \leq n \leq 7$) transition metal complexes. In the appropriate ligand field, they can exist in two different electronic states, usually referred to as high spin (HS) and low spin (LS), which exhibit sharp differences in their magnetic, optical, electrical, and mechanical properties.[4,5] Remarkably, it is possible to switch between them by applying external stimuli, such as temperature, pressure, electric fields, or light.[4] Interestingly, the spin transition can exhibit thermal hysteresis in the solid state, thus conferring bistability and memory effect on the system. SCO compounds contain all the ingredients needed to be used as binary memories since the two spin states can be addressed by applying external stimuli and read-out by sensing the changes experienced in their properties upon the spin transition. Even more, as the spin transition is molecular in nature, it may persist even at the single-molecule scale, thus permitting the development of single-molecule SCO devices. During the 1980s, the first attempts to exploit this molecular bistability in devices were reported.[6] Still, this development has been seriously limited by the loss of cooperativity at the single-molecule level, lacking memory effect, as well as by the fragility and low performance of the individual molecules. An additional challenge comes from their insulating nature in bulk. So, until very recently the use of SCO compounds as active components in electronic devices has been loosely investigated. This panorama is rapidly evolving thanks to nanotechnology. In fact, one of the current trends in Molecular Magnetism is that of integrating magnetic molecules into devices for applications in spintronics and information technologies.[3,7]

In this context, SCO memory devices have become one of the central topics in this area.[8–10] Here, an overview of the current approaches developed to exploit the SCO phenomenon in molecular electronics as well as future perspectives is showcased using SCO nanoparticles (NPs) as memory components. In the first part, we take advantage of the spin-dependent electrical conductivity showed by conveniently chosen SCO NPs to readout the spin state.[5,11] Since these nanostructures may still exhibit a cooperative spin transition, they can close the gap between the bulk and the single molecule. In fact, they behave as single molecules in terms of processability, while keeping the stability and memory effects of their bulk counterparts.[12,13] In the second part, the SCO NPs are deposited over graphene and other 2D materials. In these hybrid heterostructures, the electrical or optical changes experienced by the 2D material are used to sense the spin transition. The advantage of this approach with respect to the former one is that the insulating character of the SCO component does

R. Torres-Cavanillas, M. Gavara-Edo, E. Coronado
Instituto de Ciencia Molecular
Universitat de València
Valencia 46980, Spain
E-mail: eugenio.coronado@uv.es
R. Torres-Cavanillas
Department of Materials
Oxford University
Oxford OX2 6NN, UK

The ORCID identification number(s) for the author(s) of this article can be found under https://doi.org/10.1002/adma.202307718

DOI: 10.1002/adma.202307718

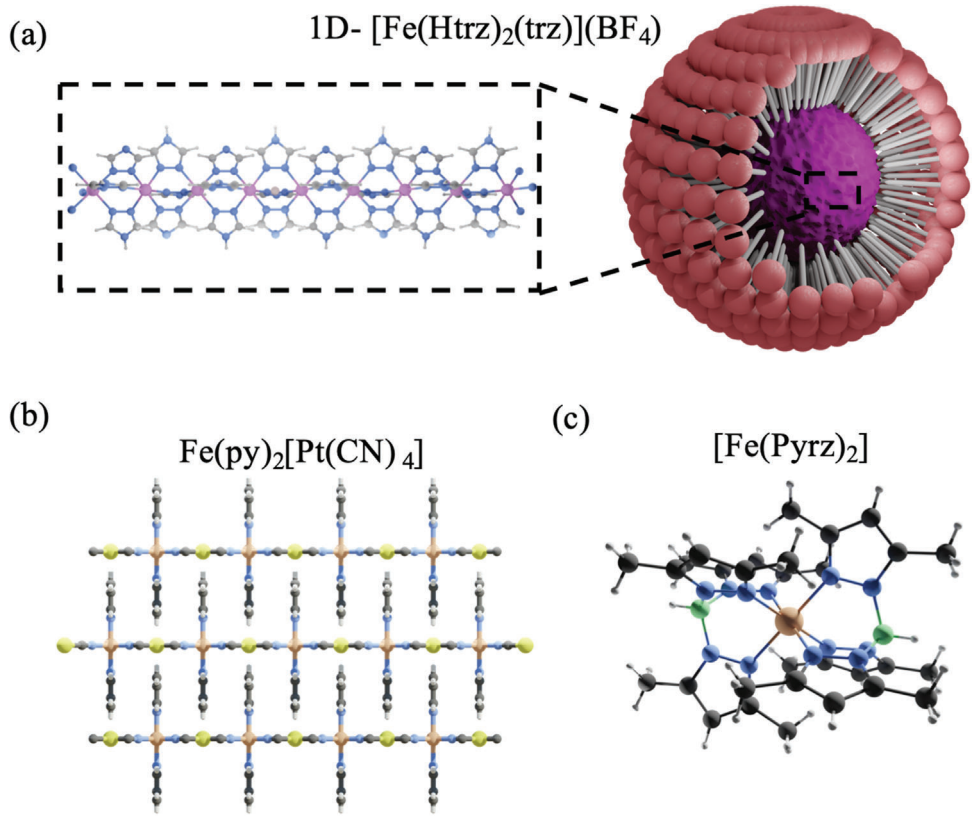

Figure 1. SCO compounds are used for electronic devices. a) $[Fe(Htrz)_2(trz)](BF_4)$, (Htrz = triazole, trz = triazolate) chain structure and micelle nanoreactor encapsulating NPs of this SCO compound; b) The Hoffmann-type layered coordination polymers $[Fe(L)_2(M(CN)_4)]$ (M = Pt, Ni; L = pyrazine or pyridine derivatives); c)The sublimable SCO molecule $[Fe(Pyrz)_2]$ (Pyrz = hydrotris-(3,5-dimethyl-pyrazolyl)borate). Blue balls are N, gray C, white H, green B, and orange Fe^{+2}.

not limit the performance of the device. In **Figure 1** we plot some relevant examples of SCO compounds that have been integrated as NPs on surfaces and in electronic devices.

2. Synthetic Protocols of Spin-Crossover NPs

The preparation of SCO NPs started in 2007 with the report of ≈10 nm NPs of $[Fe(Htrz)_2(Trz)](BF_4)$.[12] The main difficulty was to limit the growth of the SCO nanostructure while keeping its bistability, as this was the main requirement for information storage. Over the years, several protocols have been used to obtain naked SCO NPs, functionalized SCO NPs, core@shell NPs, and thin film nanocrystals grown on surfaces. In **Table 1**, a summary of these SCO nanostructures is listed.

2.1. Naked SCO NPs

These NPs are extremely desirable, as they would directly contact the electrodes. However, their synthesis has been limited to a few SCO compounds as often their growth is hardly controlled. The most obvious protocol to synthesize naked NPs is by "direct addition" of the precursors under a highly diluted concentration, forming small nucleation seeds to obtain small NPs, **Figure 2**a.[14–17] This protocol is well suited for synthesizing NPs based on non-neutral coordination polymers, ensuring colloidal stability in the resulting NPs. The primary drawback of the direct synthesis method is that it is restricted to producing small NPs (4–16 nm). To achieve larger NPs, a seed-mediated growth process is required that utilizes presynthesized NPs as nucleation seeds. However, this approach is quite complex and yields a limited quantity of the desired NPs. In this context, direct synthesis has primarily been focused on producing NPs of coordination polymers based on Prussian blue and its analogs, with a general formula $A_xM[M'(CN)_6]$ (where A = Na, K, Li, Cs, Rb; M = Fe, Mn, Ni, Cu, Co; M' = Fe, Cr). For instance, following this approach, NPs of ≈10 nm of the $CsCo[Fe(CN)_6]$ coordination polymer were reported which preserve the light-induced spin transition of the bulk (Figure 2a).[14,16,17]

A "solvent-assisted precipitation" was also used to synthesize naked NPs of monomolecular compounds, like $[Fe(NCS)_2(phen)_2]$ or $[Fe(mepy)_3tren][PF_6]_2$.[18–21] It consists of the addition of an antisolvent on a saturated solution of the SCO complex, provoking the precipitation of NPs with sizes ranging from 16 nm to microns (Figure 2b). In contrast to the direct synthesis, which is exclusive of coordination polymers, solvent-assisted precipitation is appropriate for soluble discrete molecules. Last but not least, another possibility uses a matrix that can interact with the precursors acting as a template for the

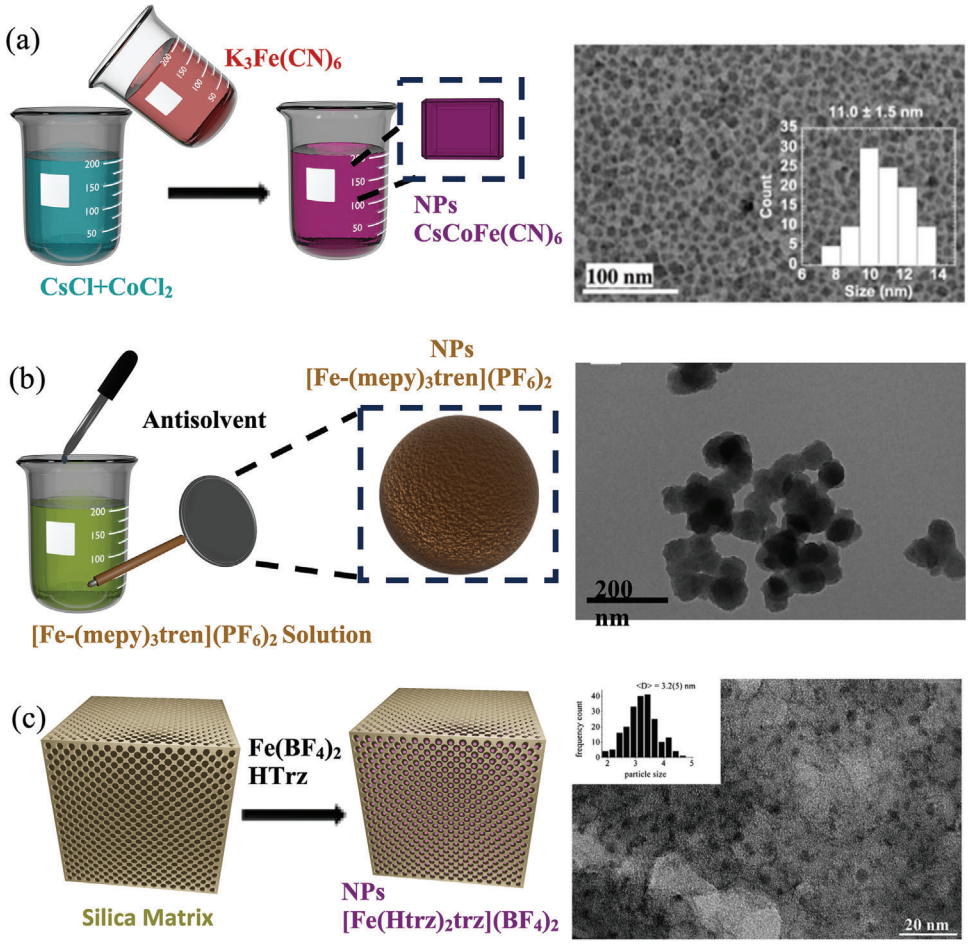

Figure 2. Synthetic protocols for the production of naked SCO NPs. a) Scheme depicting the direct synthesis of SCO NPs $CsCoFe(CN)_6$ (left), along with TEM images of 11 nm NPs of the same coordination polymer (right). b) Nanocrystals of the SCO molecule $[Fe(mepy)_3tren][PF_6]_2$, synthesized using solvent-assisted precipitation protocols; scheme on the left and TEM images on the right. c) Synthetic protocol for the synthesis of matrix-assisted SCO NPs, shown on the left, accompanied by TEM images illustrating the synthesis of 3.5 nm coordination compound $Fe(Htrz)_2(trz)$ on the right. a) Reproduced with permission.[15] Copyright 2021, MDPI. b) Reproduced with permission.[18] Copyright 2013, John Wiley and Sons. c) Reproduced with permission.[26] Copyright 2020, John Wiley and Sons.

NPs growth ("matrix-assisted synthesis") (Figure 2c).[22–27] The main problem of this protocol is that the NPs cannot be easily separated from the matrix.

2.2. Functionalized SCO NPs

The functionalization of NPs surface may be beneficial for enhancing its chemical stability and for size control. Thus, these NPs have been mainly grown using polymers or surfactants to confine them. In this context, the "reverse micelle technique" is the most widely used approach. It permits the synthesis of NPs ranging from a few to hundreds of nm by blending two separate microemulsions containing the SCO precursors stabilized by a surfactant (**Figure 3**a).[12,13,28] A control over the size and shape of the NP can be obtained by playing with some synthetic parameters like concentration, temperature, or reaction time (Figure 3b).[29–37] Especially when ionic surfactants are used, these remain at the NPs surface, enhancing their processability.[38] This was demonstrated in the compound $[Fe(HTrz)_2(Trz)](BF_4)$ for which NPs in the range 4–25 nm exhibiting a thermal hysteresis near room temperature (RT) were obtained using the surfactant AOT (Figure 3c).[12,13,29] In addition to the reverse micelle technique, the use of "hydrophobic diblock copolymers" (like polyglutamate and polyleucine) as coatings to synthesize and stabilize SCO NPs of SCO complexes has also been explored.[39–43] Note that although this procedure is very versatile and helpful in stabilizing SCO NPs, its relevance in electronic devices is minimal since the polymeric capping at the NP surface may hinder electron transport.

2.3. Core@Shell NPs

These NPs provide the opportunity to create nanoheterostructures with interesting synergies between the components and improved physical properties. In this context, the most explored example of SCO core@shell hybrid

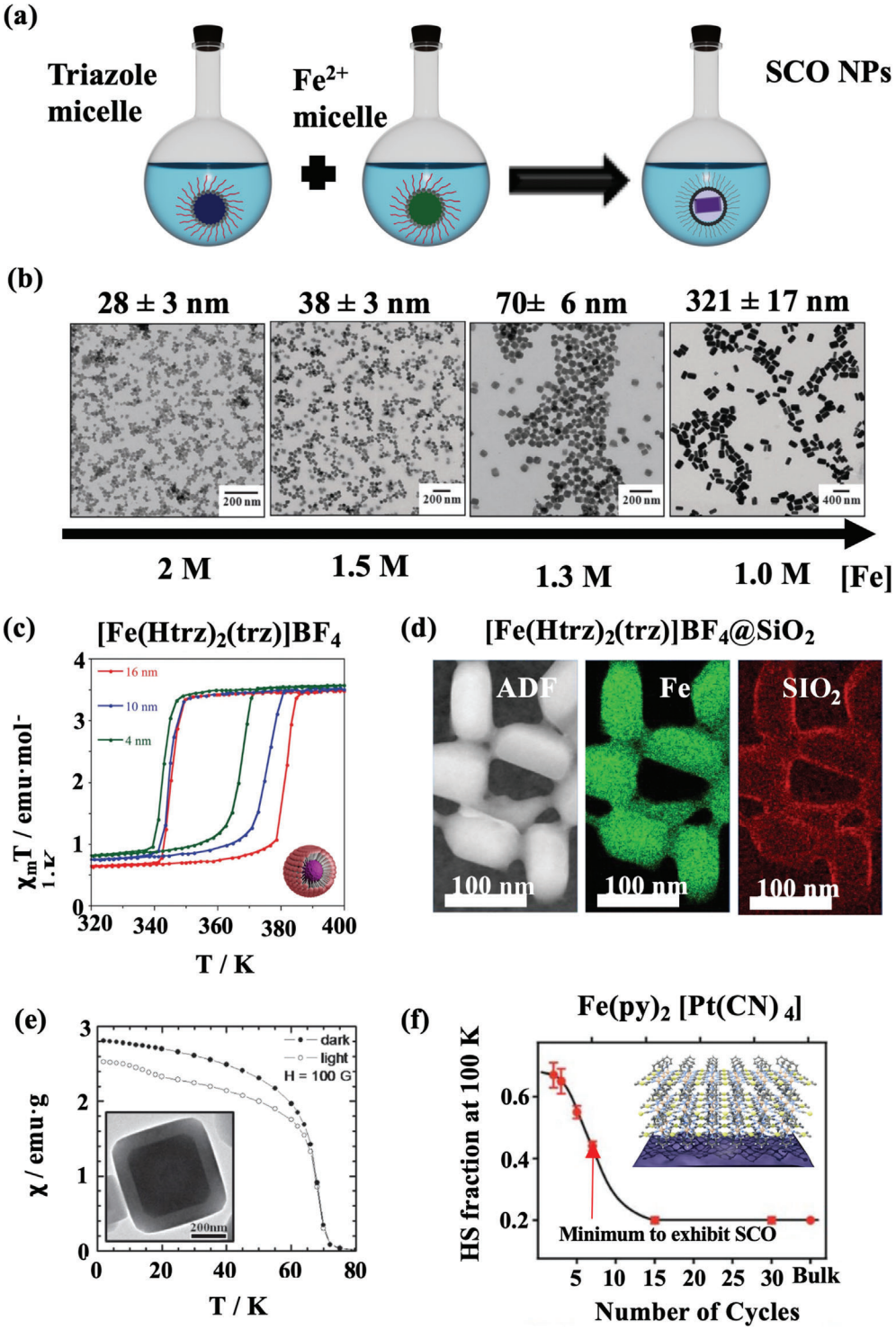

Figure 3. Results obtained on different types of SCO NPs. a) Scheme illustrating the reverse micelle technique for synthesizing SCO NPs. b) TEM images showcasing core@shell NPs of the type $[Fe(HTrz)_2(Trz)](BF_4)@SiO_2$ synthesized through the reverse micelle method, varying the concentration of precursors and reaction times. c) Size dependence of the magnetic properties for $[Fe(Htrz)_2(trz)](BF_4)$ NPs synthesized by the reverse micelle using the surfactant AOT (AOT = anionic bis(2-ethylhexyl)sulfosuccinate). d) Annular dark field TEM image and Fe and O mapping of $Fe(Htrz)_2(trz)(BF_4)@SiO_2$ NPs showing their core@shell structure.e) Magnetization as a function of the temperature of RbCoFe@KNiCr NPs before and after light irradiation. f) Ultrathin films of SCO nanocrystals grown over a gold substrate using the LBL technique. HS fraction at 100 K as a function of the number of cycles (1 cycle ≈ 0.72 nm). b,d) Reproduced with permission.[50] Copyright 2019, Royal Society of Chemistry. c) Reproduced with permission.[29] Copyright 2015, Royal Society of Chemistry. e) Reproduced with permission.[53] Copyright 2011, American Chemical Society. f) Reproduced with permission.[63] Copyright 2019, Royal Society of Chemistry.

Table 1. Summary of the different types of SCO NPs incorporated in devices and the synthetic protocols used to make them.

Type	Protocol	Nanostructured molecule	References
Naked SCO NPs	Direct addition (DA)	$\{Co[Fe(CN)_4]\}$ / DA	[14–17]
	Solvent-assisted (SA)	$[Fe(NCS)_X(L)_2]_i[Fe(mepy)_3tren][PF_6]_2$;$[Fe(III)(3\text{-}MeOSalEen)_2]PF_6$; SA	[18–21]
	Matrix-assisted (MA)	$[Fe(Htrz)_2(trz)]BF_4$ / MA	[22–26]
		$\{Fe(pz)[M(CN)_4]\}$ / MA	[27]
Functionalized SCO NPs	Reverse micelle (RM)	$[Fe(Rtrz)_3](X)_2$;$\{Fe(pz)[M(CN)_4]\}$ / RM	[12,13,28–38]
	Block copolymer and supramolecular assembly (BC)	$[Fe(L)(bipy)]_n$ $Fe(Leq)(Lax)]_n$ / BC	[39–43]
Core@shell	Reverse micelle (RM)	$Fe(pz)[Pt(CN)_4]@SiO_2$ / RM	[44]
	Seed mediated (SM)	$[Fe(Htrz)_2(trz)](BF_4)@SiO_2$ / RM	[45–51]
		$[Fe(Htrz)_2(trz)](BF_4)@[Fe(NH_2trz)_3](BF_4)$ / RM	[52]
		$Au@[Fe(Htrz)_2(trz)](BF_4)$ / SM	[58–62]
		$RbCo[Fe(CN)_6]@KNi[Cr(CN)_6]$; $RbCo[Fe(CN)_6]@KCo[Cr(CN)_6]$; $Ni[Cr(CN)_6]@Co[Fe(CN)_6]$ / SM	[53–57]
Nanocrystals on surfaces	Langmuir-Blodgett (LB)	$[Fe(L)_2M(CN)_4]$ (M = Ni, Pd, Pt, and L = pyridine, and pyrazine) / LBL	[63,70]
	Layer-by-layer (LBL)	$[Fe(C_{16}dpt)_2(NCS)_2]$, $[Fe(hpdpt)_2(SCN)_2]$, $[Fe(padpt)_2(SCN)_2]$ / LB	[67–69]
	Vacuum sublimation (VS)	$[Fe(H_2B(pz)_2)_2(phen)]$, $[Fe(HB(tz)_3)_2]$, $Fe[[Me_2Pyrz]_3BH]_2$, $[Fe(phen)_3](SCN)_2$, $[Fe\{H_2B(pz)_2\}_2(L)]$, $[Fe(Pyrz)_2]$/ VS	[62–65,71–73]

involves the coverage of SCO NPs with a silica shell.[44–46] The silica shell chemically stabilizes the SCO core by efficiently preventing iron oxidation in water, permitting its use as an MRI contrast agent,[47] or as an anchoring point to decorate NPs used as sensors.[46,48,49] Still, to be integrated in devices it is important to minimize the silica shell to a few nm, given its highly insulating character. This was achieved by modulating the kinetics of the shell formation (Figure 3d). Thus, hybrid $[Fe(Htrz)_2(trz)]BF_4@SiO_2$ NPs with a shell <3 nm were obtained,[50] and used to prepare SCO microresonators.[51]

The versatility of the reverse micelle protocol has also been exploited for preparing SCO1@SCO2 NPs (SCO1 = $[Fe(NH_2\text{-}trz)_3](BF_4)_2$ and SCO2 = $[Fe(Htrz)_2(trz)](BF_4)$),[52] or magnetic@SCO NPs (Prussian Blue Analogues over SCO $RbCo[Fe(CN)_6]$ seeds)[53–57] as exemplified in Figure 3e. In this last example, a modulation in the ferromagnetic shell magnetization was induced by the stress generated upon the light-induced spin transition of the SCO core. We recently used a seed-mediated protocol to prepare core@shell NPs formed by a metallic gold core and a SCO shell of $[Fe(Htrz)_2(trz)](BF_4)$.[58,59] The synthetic procedure relies on the functionalization of the gold NPs surface with trz that then acts as a seed for the growth of $[Fe(Htrz)_2(trz)](BF_4)$ shells ranging from 1 to 15 nm thick. This procedure was later modified by Chastanet et al. to synthesize thicker shells.[60–62]

2.4. SCO Nanocrystals Deposited on Substrates

This particular form of NPs has been grown conforming thin films.[63,64] The main synthetic approaches are the "Langmuir–Blodgett" technique (LB), the "layer-by-layer" growth (LBL), and the "vacuum sublimation" procedure (VS).[8,64–66] *LB* technique consists of the organization of amphiphilic molecules incorporating the SCO complex in a liquid–air interface to subsequently transfer the resulting monolayer onto solid substrates.[67–69] *LBL* growth is based on the alternative soaking of a substrate into solutions containing the SCO precursors and has allowed to grow polymeric Hofmann clathrate SCO compounds.[63,70] A relevant example that illustrates how the nanostructuration of these SCO coordination polymers onto solid substrates affects the spin transition was reported by Rubio et al.[63] High-quality ultrathin films of $[Fe(py)_2Pt(CN)_4]$ were fabricated, in which segregated nanocrystals of ≈25 nm (lateral size) were formed in the early stages of the growth process. These coalesced into continuous films after 10–12 cycles (≈7.6–9.1 nm thick), hindering the spin transition completeness below this thickness (Figure 3f). Finally, in the VS procedure, the SCO molecule is directly sublimed and self-assembled on flat or patterned surfaces. Hence, it is exclusive to thermally stable complexes that do not decompose during sublimation or in contact with the substrate. A remarkable example is provided by the molecule $[Fe(Pyrz)_2]$ (Figure 1c) that can be deposited over different substrates (Cu, Au) leading to organized arrays at the few-layer limit, which still exhibit thermal and light-induced SCO effects.[71–73]

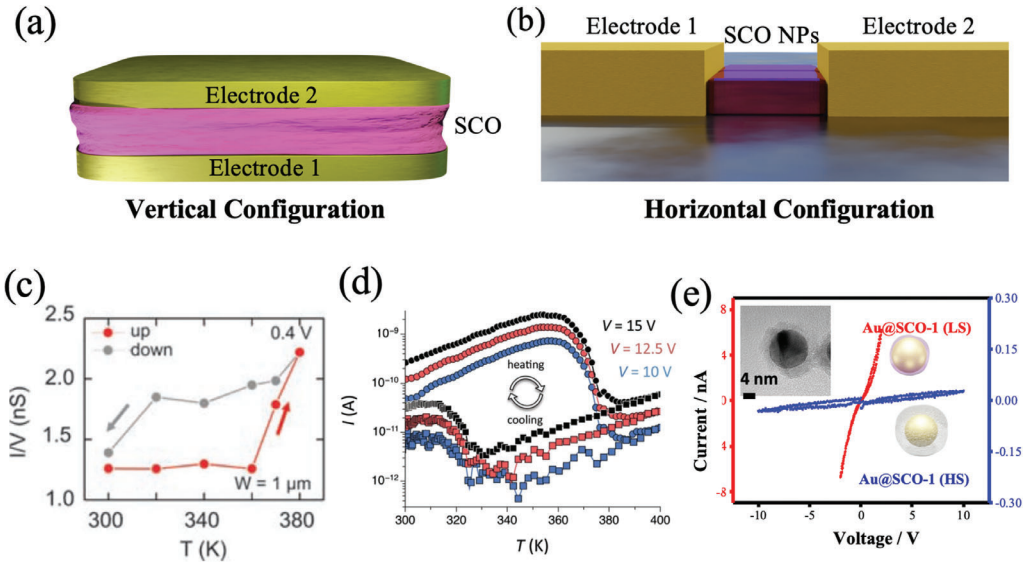

Figure 4. SCO electronic devices. Scheme of vertical a) and horizontal b) devices. c) Electrical conductivity as a function of the temperature for a 10 nm NP of $Fe(Htrz)_2(trz)(BF_4)$ placed between a nanojunction of gold electrodes with a gap of 5–10 nm. d) Electrical conductivity as a function of the temperature of microcontact printed 2D assemblies of $Fe(Htrz)_2(trz)(BF_4)$ nanorods (25 × 10 nm) interdigitated between Au electrodes with a gap of ≈50 nm. e) current versus voltage curves of the LS and HS at 350 K of a 2D-assembly of $Au@Fe(Htrz)_2(trz)(BF_4)$ (12@4 nm) core@shell NPs (inset) deposited by electrophoresis method between Au electrodes separated by a distance of 10 μm. c) Reproduced with permission.[83] Copyright 2011, John Wiley and Sons. d) Reproduced with permission.[84] Copyright 2015, John Wiley and Sons. e) Reproduced with permission.[58] Copyright 2019, John Wiley and Sons.

3. First Generation of SCO Electronic Devices: Measuring the Electrical Transport Through SCO NPs

Depending on the device's configuration, two different setups can be fabricated, namely vertical and horizontal. The vertical configuration is mainly limited to multilayer junctions encapsulating SCO sublimable complexes (**Figure 4**a).[74–78] An example is provided by 10–100 nm thick films of the SCO complex $[Fe(H_2B(pz)_2)_2(phen)]$ ($[H_2B(pz)_2]^-$ = hydrobispyrazolylborate, phen = phenantroline) sandwiched between indium tin oxide and Al electrodes.[74] In this device, the spin switching leads to a substantial and reversible change of the current intensity (up to 50%) upon the spin transition, which can be easily sensed thanks to the large area of the electrodes (3 mm^2). Remarkably, for other SCO complexes, this device configuration has afforded a very stable signal with reduced fatigue upon 10 000 successive cycles.[76] However, most vertical devices exhibit extremely low ON/OFF ratios (conductance in the high conductive state compared to the low conductive state), due to the high insulating nature of the SCO complexes, requiring either high voltages,[76,78] or the preparation of ultra-thin films,[77] increasing the risk of damaging the SCO complex or having short-circuited devices. While some authors have used liquid electrodes,[79,80] compressed pellets,[81] or embedded NPs in conductive polymers to minimize the negative effects of vertical architectures,[82] a more versatile approach is the use of horizontal junctions, where the NPs and the contacts are in the same plane (Figure 4b). This configuration permits the electrical readout of any type of nanostructure since the gap between electrodes and their nature can be tuned. Furthermore, the spin transition can be induced not only by temperature but also by light or an electrical field, expanding the possible ways to write/erase information in electronic devices.[16,61,83] However, some problems are still present that reduce the reproducibility and performance of memory devices. The most important one is again the insulating character of the SCO NPs. This often requires high voltages to detect a current and seriously compromises their stability leading to marked fatigue effects. In a series of papers, this issue has been investigated in devices based on $[Fe(Htrz)_2(trz)]BF_4$ NPs (see Figure 3c–e and **Table 2**). The choice of these bistable NPs is based on the sharp and hysteretic spin transition centered near RT exhibited by these NPs, even for very small sizes (down to 5 nm) (Figure 3c).

In a first work, an individual SCO NP (≈10 nm) in a nanojunction was measured. A reproducible hysteresis loop in the conductance centered at ≈340 K with an ON/OFF ratio of ≈3 between the low- and the high-conductance states was observed (Figure 4c).[83] Still, these devices rapidly degrade upon thermal cycling above RT and the hysteresis often disappears after the first thermal cycle.

In a second work, well-packed 2D assemblies of the SCO nanorods were placed between electrodes by microcontact printing.[84] In this case, the ON/OFF ratio was strongly improved, reaching values of ≈300 (Figure 4d); the stability was also improved, although some irreversibility in the hysteresis was observed upon successive thermal cycles, indicating some fatigue effect probably related to the loss of particle/particle or particle/electrode contacts upon the spin transition due to mechanical effects.

In a third work, we demonstrated that this stability concern could be solved by placing SCO NPs coated with a silica shell

Table 2. Representative electronic devices based on SCO NPs.

NPs	Size (nm)	Device	Gap (μm)	Conductance ON (S)	ON/OFF ratio	References
$[Fe(HTrz)_2(Trz)]$@AOT	10	Horizontal	5.10^{-3}	2.10^{-11}	3	[83]
$[Fe(HTrz)_2(Trz)]$@AOT	10 × 25	Horizontal	5.10^{-2}	8.10^{-11}	310	[84]
$[Fe(HTrz)_2(Trz)]@SiO_2$	110 × 50 (SiO_2 shell ≈ 11)	Horizontal	0.7	1.10^{-11}	7	[85]
Au@$[Fe(HTrz)_2(Trz)]$	Au core: 12; SCO shell: 4	Horizontal	10	3.10^{-9}	5300	[58]
$[Fe(H_2B(pz)_2)_2(phen)]$	10	Vertical	1.10^{-2}	2.10^{-9}	2	[74]
$[Fe(HB(tz)_3)_2]$	7	Vertical	7.10^{-3}	3.10^{-8}	100	[78]

in between graphene electrodes. A reproducible hysteresis was observed after repeating thermal cycles (up to seven without any apparent fatigue).[85] This device's resilience was attributed to the graphene flexibility, which improves the SCO/electrode contacts.

Overall, electrode gaps in the nanometre range (5–700 nm) were required in these devices to overcome the insulating nature of the NPs, enabling the detection of a current with conductance values of the order of 10^{-11} S. A way to go beyond this gap is by making the SCO NPs more conductive. This was achieved using core@shell NPs based on a metallic gold core surrounded by an ultrathin $[Fe(Htrz)_2(trz)](BF_4)$ shell and organizing them between interdigitated Au electrodes.[58] The electrical response of this device exhibited a conductance of the order of 10^{-9} S, while bare NPs of the same sizes were too insulating to permit any electron flow through this large gap (Figure 4e). In terms of performance, outstanding ON/OFF switching ratios of ≈5300 were reached, although its stability was limited to a maximum of five cycles. Finally, the light-induced heating of the plasmonic Au core was also exploited to induce the spin switching in the SCO shell. In this context, a photoconversion of the 55% of metallic centers from low-spin to high-spin upon light irradiation was achieved by Chastanet et al., in gold nanorods surrounded by a $[Fe(Htrz)_2(trz)](BF_4)$ shell.[60–62] Subsequently, we improved this result by employing gold nanostars as core, achieving a 60% photoconversion with light irradiation two orders of magnitude lower in intensity.[59]

In Table 2, some of the most relevant SCO nanodevices are presented. We can see that, taking the single-nanoparticle device as a starting point,[83] better performances have been progressively obtained by first enhancing the NP/electrode contacts,[84] then, by using flexible graphene electrodes,[85] and, more recently, by developing highly conductive heterostructures.[58]

4. Second Generation of SCO Electronic Devices: Toward Robust Devices Based on Hybrid Heterostructures Combining SCO NPs and 2D Materials

Despite the huge efforts of researchers in progressively achieving better performances in the SCO devices described above, rather low thermal cyclability is observed in most of them. As already mentioned, the main reason behind this issue deals with the mechanical stress experienced by the SCO nanomaterial as a consequence of its volume change upon the spin transition. However, the device architecture also limits its endurance. Particularly, in these devices, the electron transport goes directly through the insulating SCO component, thus requiring the application of high voltages. This feature typically degrades the SCO material. To address this fragility, an alternative approach has recently been proposed: interfacing SCO NPs with conducting or semiconducting 2D materials to form hybrid SCO/2D heterostructures. Here, the current would preferentially flow through the 2D material instead of the insulating SCO, aiming to assess the influence of the molecular component on the properties of the "all surface" 2D material. This concept, recently exploited in electronic devices based on molecular/2D heterostructures such as organic field-effect transistors (OFETs) or chemical sensors,[86,87] can be used here to sense the spin transition.

The first SCO device of this type was reported in 2017.[88] It was based on a heterostructure formed by a layer of AOT-functionalized SCO NPs of $[Fe(Htrz)_2(trz)](BF_4)$ deposited on a precontacted graphene film grown by chemical vapor deposition (CVD). A reversible change in the electrical properties of the 2D material was induced by the SCO component, sensing the thermal spin transition (**Figure 5**a). A similar approach was later followed by Dayen et al., using SCO NPs of $[Fe(Htrz)_2(trz)](PF_6)$, where the spin transition was photothermally induced and also detected through the electrical properties of the CVD-graphene in the hybrid device.[89] Next, this concept was extended to 2D semiconductors such as 2H-MoS_2.[90] In this case, the contact between the SCO NP and the 2D material was optimized by covalently bonding the two components. Thus, hybrid NPs of $[Fe(Htrz)_2(trz)](BF_4)@SiO_2$ were anchored on chemically exfoliated MoS_2 layers conveniently functionalized with a trimethoxisylane group. As a result, this heterostructure allows to sense the spin state not only electrically but also optically (Figure 5b). Particularly, the spin transition induces a strain (of ≈0.6%) over the MoS_2 layer, shifting the photoluminescence band toward lower energies as a consequence of a change in the bandgap. This optical sensing of the spin state has shown to be very sensitive to the spin transition and furthermore does not need electrodes, thereby facilitating the device architecture. However, the aforementioned procedures still require to process the materials in solution.

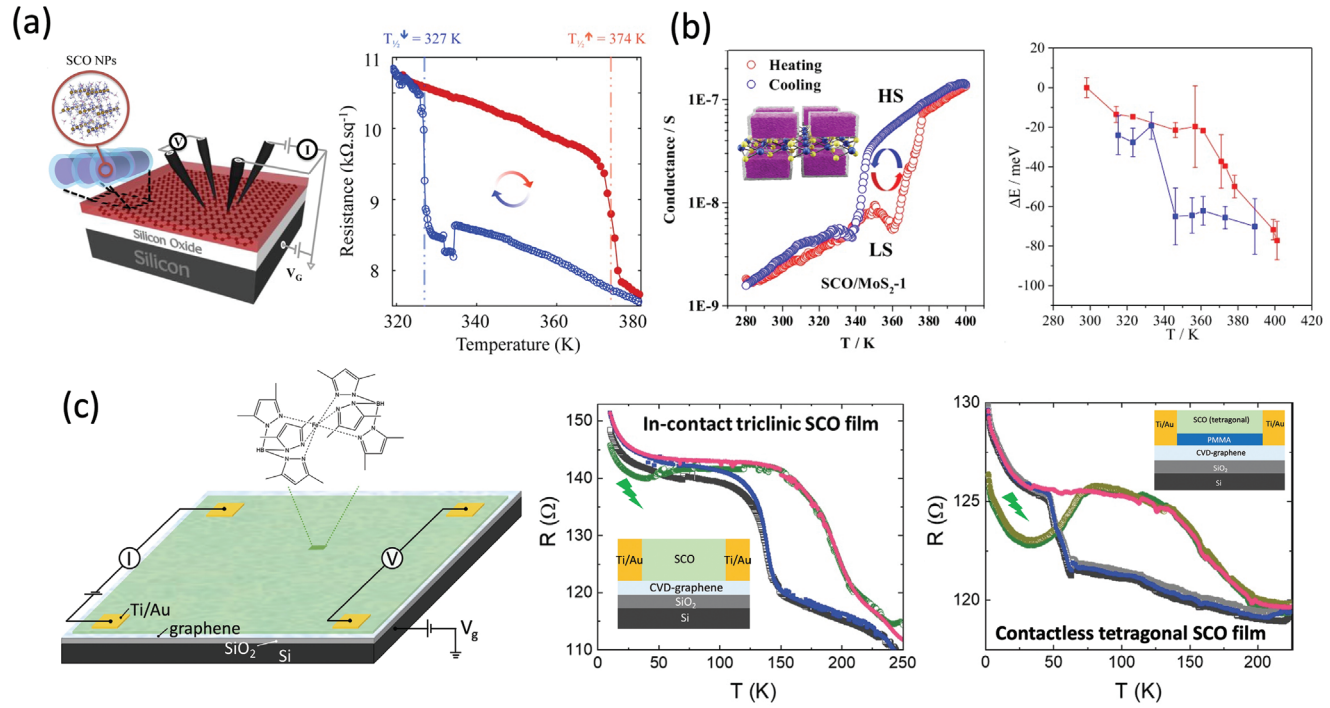

Figure 5. *SCO/2D electronic devices.*a) Schematic drawing of a FET device conformed by AOT-functionalized SCO NPs of $[Fe(Htrz)_2(trz)](BF_4)$ (25 nm long and 9 nm wide) deposited on CVD-graphene (left) and its temperature variable electrical resistance measurements (right). b) Temperature variable conductance (left) of 2H-MoS_2 flakes decorated with 70 nm long SCO $[Fe(Htrz)_2(trz)](BF_4)/SiO_2$ NPs (inset) pellet and (right) bandgap shift along the SCO NPs thermal spin transition for both cooling (blue line) and heating (red line) cycles. c) Typical device architecture used (left) and temperature variable electrical resistance measurements of (middle) an in-contact device integrating a 130 nm thick sublimed film of $[Fe(Pyrz)_2]$ in its triclinic polymorph (deposited at 100 °C) conformed by 200 nm diameter nanocrystals and directly grown on a CVD-graphene layer showing a LIESST yield of 15% after 60 min laser irradiation, and (right) a contactless device integrating a 100 nm thick film $[Fe(Pyrz)_2]$ in its tetragonal polymorph (deposited at −90 °C) conformed by 100 nm diameter nanocrystals deposited on a CVD-graphene layer with a 30 nm thick film of polymethyl methacrylate embedded between them showing a LIESST yield of 100% after 5 min laser irradiation. The measurements of both devices show various consecutively performed thermal cycles with and without laser irradiation (532 nm laser with a power of 28.2 μW mm^{-2} in contrast to the 647 nm laser with a power of 550 μW mm^{-2} used in the previous work[91]). a) Reproduced with permission.[88] Copyright 2017, American Chemical Society. b) Reproduced with permission.[90] Copyright 2021, Springer Nature. c) Reproduced with permission.[92] Copyright 2022, John Wiley and Sons.

To overcome this, a dry procedure involving the deposition of sublimable SCO complexes over CVD-graphene pre-patterned chips was developed,[91–93] since it is more compatible with the UHV techniques used in electronics. The first work was reported in 2021 by depositing crystalline thin films (≈120 nm thick) of the neutral molecule $[Fe(Pyrz)_2]$ on CVD-graphene chips.[91] These devices allowed to electrically detect the thermal SCO transition and also a light-induced one (LIESST effect). Still, the robustness and cyclability of the devices were not demonstrated, and long irradiation times (hours) with high laser powers were required to achieve a full spin transition. In a subsequent work, the device performance was sharply improved.[92] Thus, by optimizing the sublimation conditions, two different polymorphs of this sublimable molecule, triclinic and tetragonal, were selectively grown as nanocrystalline films on the graphene chips, and their transport properties were measured (Figure 5c). For the triclinic polymorph, both thermal and light-induced spin transitions were robustly detected, for several consecutive thermal cycles (up to 11), in a device formed by cohesive SCO nanocrystals in direct contact with graphene. However, only a partial LIESST effect was observed for that polymorph. The results obtained for the tetragonal polymorph were more appealing. Thus, in-contact devices of this polymorph exhibited a much faster and effective LIESST effect. Even more, by inserting a 30 nm thick flexible polymeric PMMA interlayer between both active components in a contactless configuration, the performance was further improved, allowing to reach a quantitative yield (≈100%) in only 5 min of laser irradiation. This was attributed to the elastic properties of the polymer that can facilitate the volume change of the SCO material during its photoexcitation. In addition, these devices were very robust upon both thermal cycling and aging (up to 25 cycles were studied within a 2-month period).

Overall, the combination of SCO NPs with 2D materials has been demonstrated to be a very promising approach to preparing robust SCO electronic devices. The examples reported here are only the most representative ones. Other SCO compounds, either other sublimable molecules, that grow as amorphous and homogeneous films,[93] or SCO crystals,[94,95] have also been interfaced with 2D materials. In all these examples, the 2D material is capable of acting as a reliable and highly sensitive spin state sensor, by using the changes observed in the electrical or optical properties of the 2D material to readout the spin state

and without experiencing any apparent fatigue upon thermal cycling.

5. Outlook and Perspectives

Since the pioneering proposal by Olivier Kahn in the 80′s of exploiting the optical bistability of the spin crossover phenomenon to fabricate display devices operating at RT,[6] a trend in this field has been developed to incorporate these molecular materials in electronic devices in order to electrically readout their spin state. However, as it has been shown in this work, the insulating character, chemical reactivity, and mechanical fragility of the SCO complexes have strongly limited its development. In fact, only in the last decade, the first generation of electronic devices based on the SCO phenomenon has emerged thanks to the advances made in the miniaturization of these compounds as ultrathin films and crystalline NPs of controlled size, shape, and surface functionalization. This generation is now being complemented with more robust and resilient hybrid devices in which the spin transition is electrically or optically sensed through graphene or other semiconducting 2D materials placed underneath.

Overall, this emergent field has made spectacular advances in the last few years but is still in its infancy in terms of real applications. From the fundamental point of view, these advances have raised several questions and can open new opportunities:

In terms of chemistry, a key aspect is that of expanding the number of thermally stable SCO complexes that can sublime and remain intact in contact with surfaces. Very few examples of this kind are still known, but it is even more challenging to keep and detect spin-switching effects at the single-molecule level. In this vein, some attempts to interrogate and switch the spin state of both individual and nanoscale assemblies of molecules in direct contact with surfaces have been reported using low-temperature scanning tunneling microscopy, but at best only indirect identification of the spin states has been possible.[96,97]

In terms of devices, the first issue refers to the miniaturization of these memory bits. Here the problem is to keep the memory effect in a single NP while reducing its size since the thermal hysteresis is lost at the molecular limit. In this sense, a recent report has demonstrated that an anionic iron-triazole complex can exhibit a memory effect at RT even at the single-molecule level without the need of any cooperative effect.[98] This paradigmatic shift may open new possibilities in the design of single-molecule SCO memory devices.

Another concern is related to the performance of the SCO/2D heterostructures. They have shown to be an advantageous solution to guarantee the device's endurance without being limited by the insulating character of the SCO component. However, a detailed knowledge of the interfacial interactions between the two components, both in terms of strain and electronic effects, as well as the way in which we can tune them, is now required to improve their performance. Obviously, this concept can also be extended to other 2D materials, for example, quantum ones (superconductors and magnets). Here, instead of using these 2D materials to sense the spin transition, the interest will be more focused on tuning the properties of these quantum materials through the SCO component. We can imagine for example to control the superconductivity of a 2D material with light (via the LIESST effect) or to create and manipulate magnons in a 2D magnet via the local strain induced by the SCO nanostructure.

Acknowledgements

R.T.-C. and M.G.-E. contributed equally to this work. The authors acknowledge the financial support from the European Union (ERC AdG Mol-2D 788222, FET OPEN SINFONIA 964396), the Spanish MCIN (2D-HETEROS PID2020-117152RB-100, co-financed by FEDER, and Excellence Unit "María de Maeztu" CEX2019-000919-M) and the Generalitat Valenciana (PROMETEO Program, PROMETEO/2021/022). This study forms part of the Advanced Materials program and was supported by MCIN with funding from European Union NextGenerationEU (PRTR-C17.I1) and by Generalitat Valenciana. R.T.-C. thanks the Generalitat Valenciana for his APOSTD Fellowship (CIAPOS/2021/269). M. G.-E. acknowledges the support of a fellowship FPU15/01474 from MIU.

Conflict of Interest

The authors declare no conflict of interest.

Keywords

2D materials, hybrid heterostructures, molecular memory devices, smart nanoparticles, spin-crossover complexes

Received: August 1, 2023
Revised: August 25, 2023
Published online:

[1] J.-P. Launay, M. Verdaguer, *Electrons in Molecules*, Oxford University Press, Oxford, UK, **2018**.
[2] F. Biscarini, E. Coronado, A. Painelli, M. Yamashita, *J. Mater. Chem. C* **2021**, *9*, 10521.
[3] E. Coronado, *Nat. Rev. Mater.* **2019**, *5*, 87.
[4] M. A. Halcrow, *Spin-Crossover Materials*, John Wiley & Sons Ltd, Oxford, UK, **2013**.
[5] J. Dugay, W. Evers, R. Torres-Cavanillas, M. Giménez-Marqués, E. Coronado, H S. J. Van Der Zant, *J. Phys. Chem. Lett.* **2018**, *9*, 5672.
[6] O. Kahn, C. J Martinez, *Science (80-.).* **1998**, *279*, 44.
[7] A. Gaita-Ariño, F. Luis, S. Hill, E. Coronado, *Nat. Chem.* **2019**, *11*, 301.
[8] K. S. Kumar, M. Ruben, *Angew. Chem., Int. Ed.* **2021**, *60*, 7502.
[9] V. Rubio-Giménez, S. Tatay, C. Martí-Gastaldo, *Chem. Soc. Rev.* **2020**, *49*, 5601.
[10] K. Senthil Kumar, M. Ruben, *Coord. Chem. Rev.* **2017**, *346*, 176.
[11] G. Molnár, S. Rat, L. Salmon, W. Nicolazzi, A. Bousseksou, *Adv. Mater.* **2018**, *30*, 1703862.
[12] E. Coronado, J. R. Galán-Mascarós, M. Monrabal-Capilla, J. García-Martínez, P. Pardo-Ibáñez, *Adv. Mater.* **2007**, *19*, 1359.
[13] J. R. Galán-Mascarós, E. Coronado, A. Forment-Aliaga, M. Monrabal-Capilla, E. Pinilla-Cienfuegos, M. Ceolin, *Inorg. Chem.* **2010**, *49*, 5706.
[14] L. Trinh, S. Zerdane, S. Mazérat, N. Dia, D. Dragoe, C. Herrero, E. Rivière, L. Catala, M. Cammarata, E. Collet, T. Mallah, *Inorg. Chem.* **2020**, *59*, 13153.
[15] L. Trinh, E. Rivière, S. Mazerat, L. Catala, T. Mallah, *Magnetochemistry* **2021**, *7*, 99.
[16] M. Cammarata, S. Zerdane, L. Balducci, G. Azzolina, S. Mazerat, C. Exertier, M. Trabuco, M. Levantino, R. Alonso-Mori, J M. Glownia, S. Song, L. Catala, T. Mallah, S F. Matar, E. Collet, *Nat. Chem.* **2021**, *13*, 10.

[17] S. Zerdane, M. Hervé, S. Mazerat, L. Catala, R. Alonso-Mori, J. M. Glownia, S. Song, M. Levantino, T. Mallah, M. Cammarata, E. Collet, *Faraday Discuss.* **2022**, *237*, 224.
[18] P. Chakraborty, M.-L. Boillot, A. Tissot, A. Hauser, *Angew. Chem., Int. Ed.* **2013**, *52*, 7139.
[19] J. Laisney, A. Tissot, G. Molnár, L. Rechignat, E. Rivière, F. Brisset, A. Bousseksou, M.-L. Boillot, *Dalt. Trans.* **2015**, *44*, 17302.
[20] L. L. Nguyen, R. Guillot, J. Laisney, L. Rechignat, S. Bedoui, G. Molnár, E. Rivière, M.-L. Boillot, *New J. Chem.* **2015**, *39*, 1603.
[21] A. Tissot, L. Rechignat, A. Bousseksou, M.-L. Boillot, *J. Mater. Chem.* **2012**, *22*, 3411.
[22] C. Faulmann, J. Chahine, I. Malfant, D. De Caro, B. Cormary, L. Valade, *Dalt. Trans.* **2011**, *40*, 2480.
[23] P. Durand, S. Pillet, El-E Bendeif, C. Carteret, M. Bouazaoui, H. El Hamzaoui, B. Capoen, L. Salmon, S. Hébert, J. Ghanbaja, L. Aranda, D. Schaniel, *J. Mater. Chem. C* **2013**, *1*, 1933.
[24] V. Nagy, K. Halász, M.-T. Carayon, Il' A. Gural'skiy, S. Tricard, G. Molnár, A. Bousseksou, L. Salmon, L. Csóka, *Colloids Surfaces A Physicochem. Eng. Asp.* **2014**, *456*, 35.
[25] T. Zhao, L. Cuignet, M. M. Dîrtu, M. Wolff, V. Spasojevic, I. Boldog, A. Rotaru, Y. Garcia, C. Janiak, *J. Mater. Chem. C* **2015**, *3*, 7802.
[26] G. Zoppellaro, K. CePe, C. Aparicio, J. Ugolotti, R. Zboril, *Chem. – An Asian J.* **2020**, *15*, 2637.
[27] A. Tokarev, J. Long, Y. Guari, J. Larionova, F. Quignard, P. Agulhon, M. Robitzer, G. Molnár, L. Salmon, A. Bousseksou, *New J. Chem.* **2013**, *37*, 3420.
[28] A. A. Blanco, D. J. Adams, J. D. Azoulay, L. Spinu, J. B. Wiley, *Molecules* **2022**, *27*, 1213.
[29] M. Giménez-Marqués, M. L García-Sanz De Larrea, E. Coronado, *J. Mater. Chem. C* **2015**, *3*, 7946.
[30] T. Forestier, A. Kaiba, S. Pechev, D. Denux, P. Guionneau, C. Etrillard, N. Daro, E. Freysz, J.-F. Létard, *Chem. – A Eur. J.* **2009**, *15*, 6122.
[31] A. Rotaru, F. Varret, A. Gindulescu, J. Linares, A. Stancu, J. F. Létard, T. Forestier, C. Etrillard, *Eur. Phys. J. B* **2011**, *84*, 439.
[32] H. Peng, Synthesis of Spin Crossover Micro- and Nano-Particles and Study of the Effect of Their Sizes and Morphologies on Their Bistability Properties, **2015**.
[33] I. A. Gural'skiy, G. Molnár, I. O. Fritsky, L. Salmon, A. Bousseksou, *Polyhedron* **2012**, *38*, 245.
[34] A. Grosjean, N. Daro, S. Pechev, C. Etrillard, G. Chastanet, P. Guionneau, *Eur. J. Inorg. Chem.* **2018**, *2018*, 429.
[35] L. Moulet, N. Daro, C. Etrillard, J.-F. Létard, A. Grosjean, P. Guionneau, *Magnetochemistry* **2016**, *2*, 10.
[36] A. Grosjean, N. Daro, S. Pechev, L. Moulet, C. Etrillard, G. Chastanet, P. Guionneau, *Eur. J. Inorg. Chem.* **2016**, *2016*, 1961.
[37] N. Lalioti, E. Giannopoulou, A. Charitos, J. Parthenios, O. Malina, M. Polaskova, A. Kalarakis, V. Tangoulis, *Dalt. Trans.* **2023**, *52*, 2937.
[38] D. Tanaka, N. Aketa, H. Tanaka, T. Tamaki, T. Inose, T. Akai, H. Toyama, O. Sakata, H. Tajiri, T. Ogawa, *Chem. Commun.* **2014**, *50*, 10074.
[39] O. Klimm, C. Göbel, S. Rosenfeldt, F. Puchtler, N. Miyajima, K. Marquardt, M. Drechsler, J. Breu, S. Förster, B. Weber, *Nanoscale* **2016**, *8*, 19058.
[40] C. Göbel, O. Klimm, F. Puchtler, S. Rosenfeldt, S. Förster, B. Weber, *Beilstein J. Nanotechnol.* **2017**, *8*, 1318.
[41] Y.-H. Luo, Q.-L. Liu, L.-J. Yang, Y. Sun, J.-W. Wang, C.-Q. You, B.-W. Sun, *J. Mater. Chem. C* **2016**, *4*, 8061.
[42] A. Tsubasa, S. Otsuka, T. Maekawa, R. Takano, S. Sakurai, T. J. Deming, K. Kuroiwa, *Polymer* **2017**, *128*, 347.
[43] C. Göbel, C. Hils, M. Drechsler, D. Baabe, A. Greiner, H. Schmalz, B. Weber, *Angew. Chem., Int. Ed.* **2020**, *59*, 5765.
[44] Y. Raza, F. Volatron, S. Moldovan, O. Ersen, V. Huc, C. Martini, F. Brisset, A. Gloter, O. Stéphan, A. Bousseksou, L. Catala, T. Mallah, *Chem. Commun.* **2011**, *47*, 11501.
[45] S. Titos-Padilla, J. M. Herrera, X.-W. Chen, J. J. Delgado, E. Colacio, *Angew. Chem., Int. Ed.* **2011**, *50*, 3290.
[46] J. M. Herrera, S. Titos-Padilla, S. J. A. Pope, I. Berlanga, F. Zamora, J. J. Delgado, K V. Kamenev, X. Wang, A. Prescimone, E. K. Brechin, E. Colacio, *J. Mater. Chem. C* **2015**, *3*, 7819.
[47] P. Gkolfi, D. Tsivaka, I. Tsougos, K. Vassiou, O. Malina, M. Polaskova, C. D. Polyzou, C. T. Chasapis, V. Tangoulis, *Dalt. Trans.* **2021**, *50*, 13227.
[48] I. F. Díaz-Ortega, E. L. Fernández-Barbosa, S. Titos-Padilla, S. J. A. Pope, J.-R. Jiménez, E. Colacio, J. M. Herrera, *Dalt. Trans.* **2021**, *50*, 16176.
[49] O. Kraieva, I. Suleimanov, G. Molnár, L. Salmon, A. Bousseksou, *Magnetochemistry* **2016**, *2*, 11.
[50] R. Torres-Cavanillas, L. Lima-Moya, F. D. Tichelaar, H. W. Zandbergen, M. Giménez-Marqués, E. Coronado, *Dalt. Trans.* **2019**, *48*, 15465.
[51] J. Dugay, M. Giménez-Marqués, W. J. Venstra, R. Torres-Cavanillas, U. N. Sheombarsing, N. Manca, E. Coronado, H. S. J. Van Der Zant, *J. Phys. Chem. C* **2019**, *123*, 6778.
[52] Y.-X. Wang, D. Qiu, S.-F. Xi, Z.-D. Ding, Z. Li, Y. Li, X. Ren, Z.-G. Gu, *Chem. Commun.* **2016**, *52*, 8034.
[53] M. F. Dumont, E. S. Knowles, A. Guiet, D. M. Pajerowski, A. Gomez, S. W. Kycia, M. W. Meisel, D. R. Talham, *Inorg. Chem.* **2011**, *50*, 4295.
[54] C. R. Gros, M. K. Peprah, A. C. Felts, T. V. Brinzari, O. N. Risset, J. M. Cain, C. F. Ferreira, M. W. Meisel, D. R. Talham, *Dalt. Trans.* **2016**, *45*, 16624.
[55] A. C. Felts, A. Slimani, J. M. Cain, M. J. Andrus, A. R. Ahir, K. A. Abboud, M. W. Meisel, K. Boukheddaden, D. R. Talham, *J. Am. Chem. Soc.* **2018**, *140*, 5814.
[56] O. N. Risset, T. V. Brinzari, M. W. Meisel, D. R. Talham, *Chem. Mater.* **2015**, *27*, 6185.
[57] O. N. Risset, P. A. Quintero, T. V. Brinzari, M. J. Andrus, M. W. Lufaso, M. W. Meisel, D. R. Talham, *J. Am. Chem. Soc.* **2014**, *136*, 15660.
[58] R. Torres-Cavanillas, R. Sanchis-Gual, J. Dugay, M. Coronado-Puchau, M. Giménez-Marqués, E. Coronado, *Adv. Mater.* **2019**, *31*, 1900039.
[59] R. Sanchis-Gual, R. Torres-Cavanillas, M. Coronado-Puchau, M. Giménez-Marqués, E. Coronado, *J. Mater. Chem. C* **2021**, *9*, 10811.
[60] M. Palluel, N. M. Tran, N. Daro, S. Buffière, S. Mornet, E. Freysz, G. Chastanet, *Adv. Funct. Mater.* **2020**, *30*, 2000447.
[61] Y. Hu, M. Picher, N. M. Tran, M. Palluel, L. Stoleriu, N. Daro, S. Mornet, C. Enachescu, E. Freysz, F. Banhart, G. Chastanet, *Adv. Mater.* **2021**, *33*, 2105586.
[62] N. M. Tran, M. Palluel, N. Daro, G. Chastanet, E. Freysz, *J. Phys. Chem. C* **2021**, *125*, 22611.
[63] V. Rubio-Giménez, C. Bartual-Murgui, M. Galbiati, A. NunEz-López, J. Castells-Gil, B. Quinard, P. Seneor, E. Otero, P. Ohresser, A. Cantarero, E. Coronado, J. A. Real, R. Mattana, S. Tatay, C. Martí-Gastaldo, *Chem. Sci.* **2019**, *10*, 4038.
[64] K. S. Kumar, M. Studniarek, B. Heinrich, J. Arabski, G. Schmerber, M. Bowen, S. Boukari, E. Beaurepaire, J. Dreiser, M. Ruben, *Adv. Mater.* **2018**, *30*, 1705416.
[65] X. Zhang, P. S. Costa, J. Hooper, D. P. Miller, A. T. N'diaye, S. Beniwal, X. Jiang, Y. Yin, P. Rosa, L. Routaboul, M. Gonidec, L. Poggini, P. Braunstein, B. Doudin, X. Xu, A. Enders, E. Zurek, P. A. Dowben, *Adv. Mater.* **2017**, *29*, 1702257.
[66] V. Shalabaeva, S. Rat, M. D. Manrique-Juarez, A.-C. Bas, L. Vendier, L. Salmon, G. Molnár, A. Bousseksou, *J. Mater. Chem. C* **2017**, *5*, 4419.
[67] R. Dong, M. Pfeffermann, H. Liang, Z. Zheng, X. Zhu, J. Zhang, X. Feng, *Angew. Chem., Int. Ed.* **2015**, *54*, 12058.
[68] H. L. C. Feltham, C. Johnson, A. B. S. Elliott, K. C. Gordon, M. Albrecht, S. Brooker, *Inorg. Chem.* **2015**, *54*, 2902.
[69] J. A. Kitchen, N. G. White, C. Gandolfi, M. Albrecht, G. N. L. Jameson, J. L. Tallon, S. Brooker, *Chem. Commun.* **2010**, *46*, 6464.

[70] S. Sakaida, T. Haraguchi, K. Otsubo, O. Sakata, A. Fujiwara, H. Kitagawa, *Inorg. Chem.* **2017**, *56*, 7606.
[71] M. Kelai, V. Repain, A. Tauzin, W. Li, Y. Girard, J. Lagoute, S. Rousset, E. Otero, P. Sainctavit, M.-A. Arrio, M.-L. Boillot, T. Mallah, C. Enachescu, A. Bellec, *J. Phys. Chem. Lett.* **2021**, *12*, 6152.
[72] L. Zhang, Y. Tong, M. Kelai, A. Bellec, J. Lagoute, C. Chacon, Y. Girard, S. Rousset, M.-L. Boillot, E. Rivière, T. Mallah, E. Otero, M.-A. Arrio, P. Sainctavit, V. Repain, *Angew. Chemie Int. Ed.* **2020**, *59*, 13341.
[73] M. Kelai, A. Tauzin, A. Railean, V. Repain, J. Lagoute, Y. Girard, S. Rousset, E. Otero, T. Mallah, M.-L. Boillot, C. Enachescu, A. Bellec, *J. Phys. Chem. Lett.* **2023**, *14*, 1949.
[74] C. Lefter, S. Rat, J. S. Costa, M. D. Manrique-Juárez, C. M. Quintero, L. Salmon, I. Séguy, T. Leichle, L. Nicu, P. Demont, A. Rotaru, G. Molnár, A. Bousseksou, *Adv. Mater.* **2016**, *28*, 7508.
[75] K. Ridier, A.-C. Bas, Y. Zhang, L. Routaboul, L. Salmon, G. Molnár, C. Bergaud, A. Bousseksou, *Nat. Commun.* **2020**, *11*, 3611.
[76] Y. Zhang, L. Zhang, K. Ridier, L. Salmon, I. Séguy, G. Molnár, A. Bousseksou, *Mater. Adv.* **2022**, *3*, 8193.
[77] L. Poggini, M. Gonidec, R. K. Canjeevaram Balasubramanyam, L. Squillantini, G. Pecastaings, A. Caneschi, P. Rosa, *J. Mater. Chem. C* **2019**, *7*, 5343.
[78] Y. Zhang, I. Séguy, K. Ridier, V. Shalabaeva, M. Piedrahita-Bello, A. Rotaru, L. Salmon, G. Molnár, A. Bousseksou, *J. Phys. Condens. Matter.* **2020**, *32*, 214010.
[79] L. Poggini, M. Gonidec, J. H. González-Estefan, G. Pecastaings, B. Gobaut, P. Rosa, *Adv. Electron. Mater.* **2018**, *4*, 1800204.
[80] S. K. Karuppannan, A. Martín-Rodríguez, E. Ruiz, P. Harding, D. J. Harding, X. Yu, A. Tadich, B. Cowie, D. Qi, C. A. Nijhuis, *Chem. Sci.* **2021**, *12*, 2381.
[81] A.-C. Gheorghe, Y. S. Bibik, O. I. Kucheriv, D. D. Barakhtii, M.-V. Boicu, I. Rusu, A. Diaconu, I. A. Gural'skiy, G. Molnár, A. Rotaru, *Magnetochemistry* **2020**, *6*, 31.
[82] D. Nieto-Castro, F. A. Garcés-Pineda, A. Moneo-Corcuera, I. Sánchez-Molina, J. R. Galán-Mascarós, *Adv. Funct. Mater.* **2021**, *31*, 2102469.
[83] F. Prins, M. Monrabal-Capilla, E. A. Osorio, E. Coronado, H. S. J. Van Der Zant, *Adv. Mater.* **2011**, *23*, 1545.
[84] J. Dugay, M. Giménez-Marqués, T. Kozlova, H. W. Zandbergen, E. Coronado, H. S. J. Van Der Zant, *Adv. Mater.* **2015**, *27*, 1288.
[85] A. Holovchenko, J. Dugay, M. Giménez-Marqués, R. Torres-Cavanillas, E. Coronado, H. S. J. Van Der Zant, *Adv. Mater.* **2016**, *28*, 7228.
[86] D. Jariwala, T. J. Marks, M. C. Hersam, *Nat. Mater.* **2017**, *16*, 170.
[87] C. Anichini, W. Czepa, D. Pakulski, A. Aliprandi, A. Ciesielski, P. Samorì, *Chem. Soc. Rev.* **2018**, *47*, 4860.
[88] J. Dugay, M. Aarts, M. Giménez-Marqués, T. Kozlova, H. W. Zandbergen, E. Coronado, H. S. J. Van Der Zant, *Nano Lett.* **2017**, *17*, 186.
[89] J.-F. Dayen, N. Konstantinov, M. Palluel, N. Daro, B. Kundys, M. Soliman, G. Chastanet, B. Doudin, *Mater. Horiz.* **2021**, *8*, 2310.
[90] R. Torres-Cavanillas, M. Morant-Giner, G. Escorcia-Ariza, J. Dugay, J. Canet-Ferrer, S. Tatay, S. Cardona-Serra, M. Giménez-Marqués, M. Galbiati, A. Forment-Aliaga, E. Coronado, *Nat. Chem.* **2021**, *13*, 1101.
[91] N. Konstantinov, A. Tauzin, U. N. Noumbé, D. Dragoe, B. Kundys, H. Majjad, A. Brosseau, M. Lenertz, A. Singh, S. Berciaud, M.-L. Boillot, B. Doudin, T. Mallah, J.-F. Dayen, *J. Mater. Chem. C* **2021**, *9*, 2712.
[92] M. Gavara-Edo, R. Córdoba, F. J. Valverde-Muñoz, J. Herrero-Martín, J. A. Real, E. Coronado, *Adv. Mater.* **2022**, *34*, 2202551.
[93] M. Gavara-Edo, F. J. Valverde-Muñoz, R. Córdoba, M. C Muñoz, J. Herrero-Martín, J. A. Real, E. Coronado, *J. Mater. Chem. C* **2023**, *11*, 8107.
[94] E. P. Van Geest, K. Shakouri, W. Fu, V. Robert, V. Tudor, S. Bonnet, G. F. Schneider, *Adv. Mater.* **2020**, *32*, 1903575.
[95] C. Boix-Constant, V. García-López, E. Navarro-Moratalla, M. Clemente-León, J. L. Zafra, J. Casado, F. Guinea, S. Mañas-Valero, E. Coronado, *Adv. Mater.* **2022**, *34*, 2110027.
[96] S. Johannsen, S. Ossinger, J. Grunwald, A. Herman, H. Wende, F. Tuczek, M. Gruber, R. Berndt, *Angew. Chemie* **2022**, *61*, e202115892.
[97] M. Gruber, R. Berndt, *Magnetochemistry* **2020**, *6*, 35.
[98] A. Moneo-Corcuera, D. Nieto-Castro, J. Cirera, V. Gómez, J. Sanjosé-Orduna, C. Casadevall, G. Molnár, A. Bousseksou, T. Parella, J. M. Martínez-Agudo, J. Lloret-Fillol, M. H. Pérez-Temprano, E. Ruiz, J. R. Galán-Mascarós, *Chem* **2023**, *9*, 377.

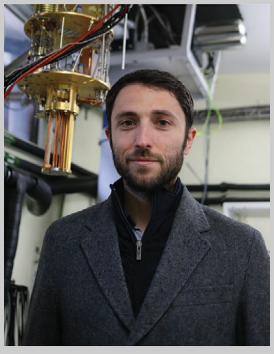

Ramón Torres-Cavanillas performed a Ph.D. thesis at the Institute for Molecular Science of the University of Valencia (ICMol) on spin crossover nanostructures under the supervision of Prof. E. Coronado. He is currently working as a postdoctoral fellow at the Department of Materials of the University of Oxford (United Kingdom) under the supervision of Prof. L. Bogani, where his research focuses on the development of novel 2D materials of interest in spintronics and optics.

Miguel Gavara-Edo performed a Ph.D. thesis at the Institute for Molecular Science of the University of Valencia (ICMol) on the chemical vapor deposition (CVD) growth of ultrathin crystals of 2D magnetic MOFs and on the fabrication of hybrid electronic devices based on sublimable spin-crossover molecules deposited over CVD graphene under the supervision of Prof. E. Coronado. Currently, he is continuing this research in the same group as a postdoctoral research associate.

Eugenio Coronado is the director of the Institute for Molecular Science (ICMol) at the University of Valencia. Expert in *Molecular Magnetism*, his current research focuses on the chemical design and processing of magnetic molecules, molecule-based magnets, and hybrid molecular/2D heterostructures combining magnetic molecules with graphene and other 2D materials for molecular electronics and spintronics.